EEET ECOLOGICAL ENGINEERING & ENVIRONMENTAL TECHNOLOGY

Ecological Engineering & Environmental Technology, 2026, 27(4), 49–64
https://doi.org/10.12912/27197050/218438
ISSN 2719–7050, License CC-BY 4.0

Received: 2026.02.04
Accepted: 2026.03.16
Published: 2026.04.01

Assessment of land cover changes before and after the September 8, 2023, Al Haouz earthquake using geoinformatics in Taroudant province, Morocco

Siham Bouzian[1*], Abdelkader Larabi[1]

[1] Water and Natural Resources Analysis and Modeling Team (WNRAM), Mohammadia School of Engineering, Mohammed V University, P.B. 765, Ibn Sina Ave., Agdal-Rabat, Morocco
* Corresponding author's e-mail: siham.bouzian@research.emi.ac.ma

ABSTRACT

Natural disasters constitute a major global challenge due to their profound impacts on land cover dynamics and natural resources. On 8 September 2023, a magnitude 6.8 earthquake struck the High Atlas region of Morocco, causing extensive human and material losses, particularly in the province of Taroudant. This study investigates land cover changes before and after the Al Haouz earthquake using an integrated remote sensing and geographic information system (GIS) framework. Multispectral Sentinel-2 imagery was employed to compute the normalized difference vegetation index (NDVI) and the normalized difference water index (NDWI) in order to quantify vegetation and surface water dynamics. A supervised maximum likelihood classification was further applied to map and compare the spatial distribution of five land cover classes, water bodies, vegetation, greenhouses, built-up areas, and bare land, across pre- and post-seismic periods. To contextualize these changes within the geo-environmental setting, thematic layers including elevation, geological facies, fault networks, and surface and groundwater resources were generated and integrated into the spatial analysis. The results reveal a marked decline in vegetated areas, an expansion of built-up surfaces, and a significant increase in mapped water bodies following the earthquake. These spatial patterns suggest substantial post-seismic environmental reorganization, likely influenced by geomorphological instability and hydrological redistribution. The integration of land cover, hydrological, and geological datasets provides new insights into territorial resilience mechanisms in seismically active regions. Our findings highlight the critical importance of incorporating hydrogeological considerations into post-earthquake recovery strategies and land management planning. This multidisciplinary approach offers a robust scientific basis for ecological restoration, risk-informed spatial planning, and sustainable water resource management in earthquake-affected areas.

Keywords: remote sensing, GIS, geoinformatics, Al Haouz earthquake, land cover change, water resources, Taroudant, Morocco.

INTRODUCTION

Natural disasters exert profound impacts on both physical and human environments by altering landscape structure, ecosystem functioning, and socio-economic systems. Among these hazards, earthquakes represent particularly disruptive events due to their sudden onset and capacity to trigger rapid and often irreversible land cover (LC) transformations. Land cover, defined as the physical and biological cover of the Earth's surface, including vegetation, water bodies, bare soil, and built-up areas, plays a central role in ecosystem services, resource management, and territorial planning. Monitoring spatial and temporal LC dynamics is therefore essential for understanding environmental change and supporting post-disaster recovery strategies.

On 8 September 2023, a magnitude 6.8 earthquake struck the Al Haouz region of Morocco, severely affecting large parts of the province of Taroudant. According to national assessments,

approximately 64% of the province experienced varying degrees of impact. Beyond the immediate destruction of infrastructure and settlements, the earthquake likely induced substantial modifications in hydrographic networks, irrigated areas, slope stability, and vegetation cover. Such transformations may influence long-term geomorphological and hydrological processes, thereby reshaping the territorial system.

Remote sensing and geographic information systems (GIS), collectively referred to as geoinformatics, provide powerful tools for detecting and quantifying land cover changes across multiple temporal scales. Multispectral satellite imagery enables the computation of spectral indices such as the normalized difference vegetation index (NDVI) and the normalized difference water index (NDWI), which are widely applied to monitor vegetation health and surface water dynamics. While previous earthquake-related studies have primarily focused on seismic mechanisms, landslide mapping, and hazard assessment, comparatively limited research has undertaken detailed pre- and post-event land cover quantification using high-resolution satellite imagery to evaluate landscape-scale transformations.

This study addresses this gap by conducting a comprehensive spatio-temporal assessment of land cover dynamics in Taroudant province before and after the 2023 earthquake. Using Sentinel-2 imagery with 10-m spatial resolution, we generated a post-disaster land cover map for 2024 and compared it with pre-event conditions through spectral index analysis and supervised classification. The methodological framework integrates geomorphological, hydrogeological, and seismic datasets to contextualize observed LC transitions within the broader geo-environmental system.

We test two central hypotheses: (1) the earthquake triggered statistically significant land cover changes across the province, and (2) vegetation and built-up areas represent the most affected categories. By combining land cover mapping with geological and hydrological information, this study provides an integrated perspective on post-seismic landscape reorganization. The results contribute to improving dynamic environmental monitoring in earthquake-prone regions and offer a scientific basis for ecosystem restoration, spatial planning, and sustainable resource management under conditions of increasing environmental risk.-affected areas.

MATERIALS AND METHODS

This study assessed land cover changes in the Taroudant Province before and after the Al Haouz earthquake of September 8, 2023, using remote sensing and GIS.

Study area

The Taroudant Province is located in southwest Morocco, between latitudes 29°70’ and 31°11’ N and longitudes 9°6’ and 7°47’ W (Figure 1). Although the climate in this region is semi-arid to sub-desert, it is protected from the effects of the desert by the Atlantic Ocean current and the Anti-Atlas mountain range. The average annual rainfall on the plain is 200 mm, which is low and erregular. The average annual temperature was almost 19 °C, the average maximum temperature was 27 °C, and the lowest temperature was 11 °C.

The province of Taroudant is located in the centre of the Souss-Massa region and covers an area of 16 500 km^2. According to the 2024 general population and housing census, it has a population of 858 162 inhabitants, which is the most populous province in the Souss Massa region. The province currently has 89 rural municipalities and 8 urban municipalities. The provincial capital is the city of Taroudant.

The province’s territory is characterised by its geographical diversity, it is composed of 40% of the Souss plain and 60% of the High Atlas and Anti-Atlas mountain ranges.

Datasets

- Satellite imagery: Sentinel-2 Level-2A, images (10 m spatial resolution) for pre-earthquake acquired in August 2023 and post-earthquake acquired in September 2024 periods were downloaded from the USGS Earth Explorer platform. These images were used for land cover classification and for the computation of NDVI and NDWI indices.
- Topographic data: A digital elevation model (DEM) of the study area was created by mosaicking available tiles covering the Taroudant Province.
- Thematic data: The geological map of Morocco (scale 1:1,000,000) and administrative boundary maps were obtained from the Geological Service of Morocco and the national geoportal (maps.geojamal.com).

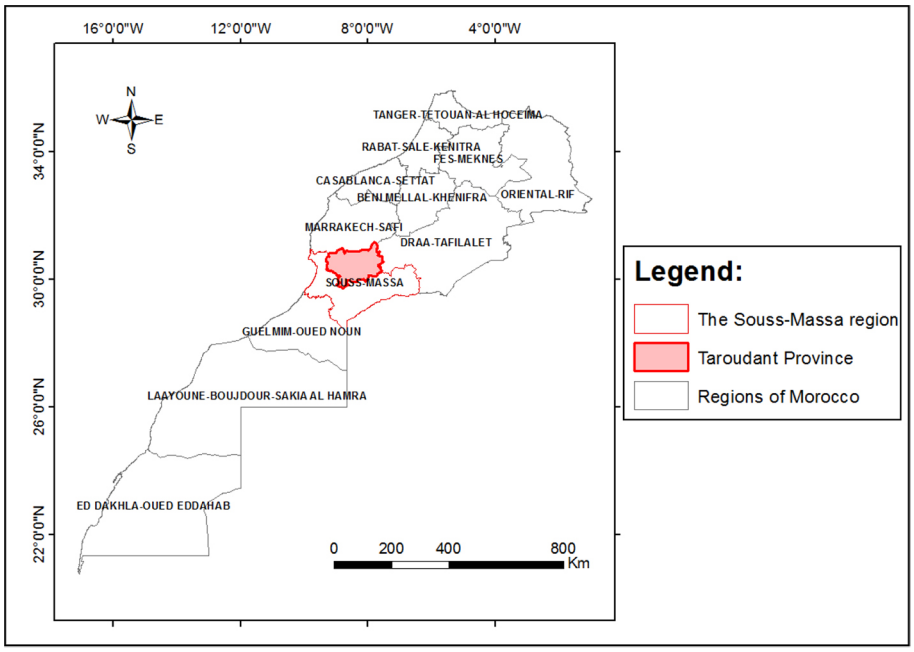

Figure 1. Location map of the study site

Preprocessing of satellite data

Preprocessing steps ensured geometric and spatial consistency between datasets.

- Mosaicking: Multiple Sentinel-2 tiles covering Taroudant Province were mosaicked using ArcGIS and QGIS software to create a single continuous image.
- Geometric correction: All datasets were aligned to the WGS-84/UTM Zone 29N coordinate system.
- Subsetting: The datasets were clipped according to the administrative boundaries of Taroudant Province.

Thematic data generation

Thematic layers were produced to ameliorate spatial analysis and interpretation:

- Hydrographic network and watershed boundarie were generated from the DEM using ArcGIS hydrology tools (Figure 2a).
- Geological faults and lithological facies were manually digitized from the geological map (Figure 2b) to improve spatial correlation with land cover change results.

Vegetation and water index analysis

To quantify vegetation and surface water dynamics, the normalized difference vegetation index (NDVI) and the normalized difference water index (NDWI) were computed for both pre- and post-earthquake Sentinel-2 scenes (Figure 2c). All calculations were performed using atmospherically corrected surface reflectance data to ensure inter-date comparability.

NDVI was calculated using the normalized difference between the near-infrared (NIR, Band 8) and red (Band 4) bands of Sentinel-2 imagery, according to the standard formula:

$$NDVI = Index\ (NIR, RED) = \\ = \frac{NIR-RED}{NIR+RED} \quad (1)$$

This index enhances vegetation signals by exploiting the contrast between strong chlorophyll absorption in the red region and high reflectance in the near-infrared region. NDVI values range from −1 to +1, where values approaching +1 indicate dense and healthy vegetation, values around zero correspond to bare soil or sparsely vegetated surfaces, and negative values generally represent water bodies, shadows, or built-up areas.

NDWI was derived using the green (Band 3) and near-infrared (Band 8) bands as follows:

$$\frac{G - NIR}{G + NIR} \quad (2)$$

NDWI enhances open water features by emphasizing differences between green reflectance and near-infrared absorption in water bodies, thereby facilitating detection of surface water extent.

To assess earthquake-induced changes, difference maps (ΔNDVI and ΔNDWI) (Figure 2d) were generated by subtracting pre-earthquake index values from post-earthquake values on a pixel-by-pixel basis (Equation (5)).

$$\Delta Index = Index_{\text{post-earthquake}} - Index_{\text{pre-earthquake}} \quad (3)$$

A positive ΔIndex means that the surface water or vegetation content increased after the earthquake, while a negative value means the surface water or vegetation decreased.

Land cover classification and accuracy assessment

Land cover (LC) maps were generated for pre- and post-earthquake periods using multispectral imagery acquired from the Sentinel-2 mission at 10-m spatial resolution (Figure 2e). Level-1C products were atmospherically corrected to surface reflectance using the Sen2Cor processor to ensure radiometric consistency between acquisition dates. All images were co-registered and resampled where necessary to guarantee spatial alignment prior to classification.

A supervised classification approach was implemented using the maximum likelihood classifier (MLC) algorithm within the ENVI software environment. The MLC was selected due to its robustness and widespread application in multispectral image analysis, as it assumes a normal distribution of spectral signatures and assigns pixels to the class with the highest probability based on class-specific statistical parameters (mean vectors and covariance matrices).

Training samples were carefully selected to ensure spectral representativeness and class separability. Regions of interest (ROIs) were defined using a combination of field knowledge, visual interpretation of false-color composites, NDVI and NDWI thresholding, and ancillary thematic layers (geological and hydrographic maps). To minimize spectral confusion, homogeneous training areas were delineated for each class, and their statistical separability was evaluated prior to final classification.

Five primary land cover classes were identified: (1) Vegetation, (2) Barren land, (3) Urban/built-up areas, (4) Water bodies, and (5) Greenhouses. These categories were selected based on their ecological and socio-economic relevance in the province of Taroudant and their expected sensitivity to seismic disturbance.

Classification accuracy was assessed using an error (confusion) matrix derived from independent validation samples. Reference data were obtained through visual interpretation of high-resolution imagery from Google Earth and cross-checked with available ancillary datasets. From the confusion matrix, overall accuracy (OA), producer's accuracy (PA), user's accuracy (UA), and the Kappa coefficient were computed to evaluate classification performance and agreement beyond chance (Canters, 1997; Clark, 2010).The Kappa statistic was used as a complementary metric to quantify the reliability of the classification results, particularly in the presence of class imbalance (Tung et al., 1988).

This accuracy assessment framework ensured the statistical robustness of the generated LC maps and provided a reliable basis for subsequent spatio-temporal change detection analysis.

Change detection analysis

Post-earthquake land cover dynamics were assessed through a post-classification comparison between pre- and post-event LC maps. This approach enabled a pixel-wise evaluation of transitions among five primary land cover categories (Vegetation, Barren land, Urban/built-up, Water bodies, and Greenhouses), facilitating the quantification of landscape transformations induced by seismic activity.

To contextualize these changes within the broader geo-environmental framework, multiple ancillary datasets were integrated, including geomorphological, stratigraphic, and geological information. Drainage networks, slope gradients, and terrain morphology were analyzed using a high-resolution digital elevation model (DEM) to assess the influence of seismic-induced ground motion on topographically sensitive areas. Stratigraphic and lithological data were incorporated to evaluate subsurface stability, supporting the identification of zones potentially susceptible to soil liquefaction, landslides, or enhanced ground shaking. These datasets were cross-referenced with historical seismicity and geophysical measurements to reconstruct the geotechnical and tectonic context of the study area.

The LC change detection results were further interpreted in conjunction with topographic and geological layers to delineate areas at higher

risk of earthquake-induced damage. For example, built-up structures located on unconsolidated sediments or steep slopes were identified as potentially more vulnerable than those on stable bedrock. Vegetation loss and expansion of bare or built-up land were analyzed as indicators of post-seismic environmental disturbance, whereas changes in water bodies were assessed in relation to terrain depressions and slope modifications.

This integrative methodology provides a rigorous spatial framework for linking observed land cover transitions with underlying geomorphological, stratigraphic, and geological conditions. The resulting analysis supports both hazard assessment and post-disaster planning, including prioritization of emergency interventions, evaluation of infrastructure vulnerability, and guidance for sustainable reconstruction and land management in the province of Taroudant.

RESULTS AND DISCUSSION

Morpho-structural

The Taroudant province is characterized by a complex morphostructural setting shaped by the interaction of tectonic and geological processes. The province is located at the convergence of the Anti-Atlas and High Atlas mountain ranges, both of which significantly influence its topography (Figure 3).

Tectonic activity, particularly during Alpine orogeny, contributed to the uplift of the Atlas Mountains and the subsidence of the Souss-Massa basin. The region is also seismically active, with periodic earthquakes caused by movements along the fault zones. Erosion and sedimentation processes also contribute to the dynamism of the province's landscape, with river systems such as the Souss playing an important role in shaping the landscape.

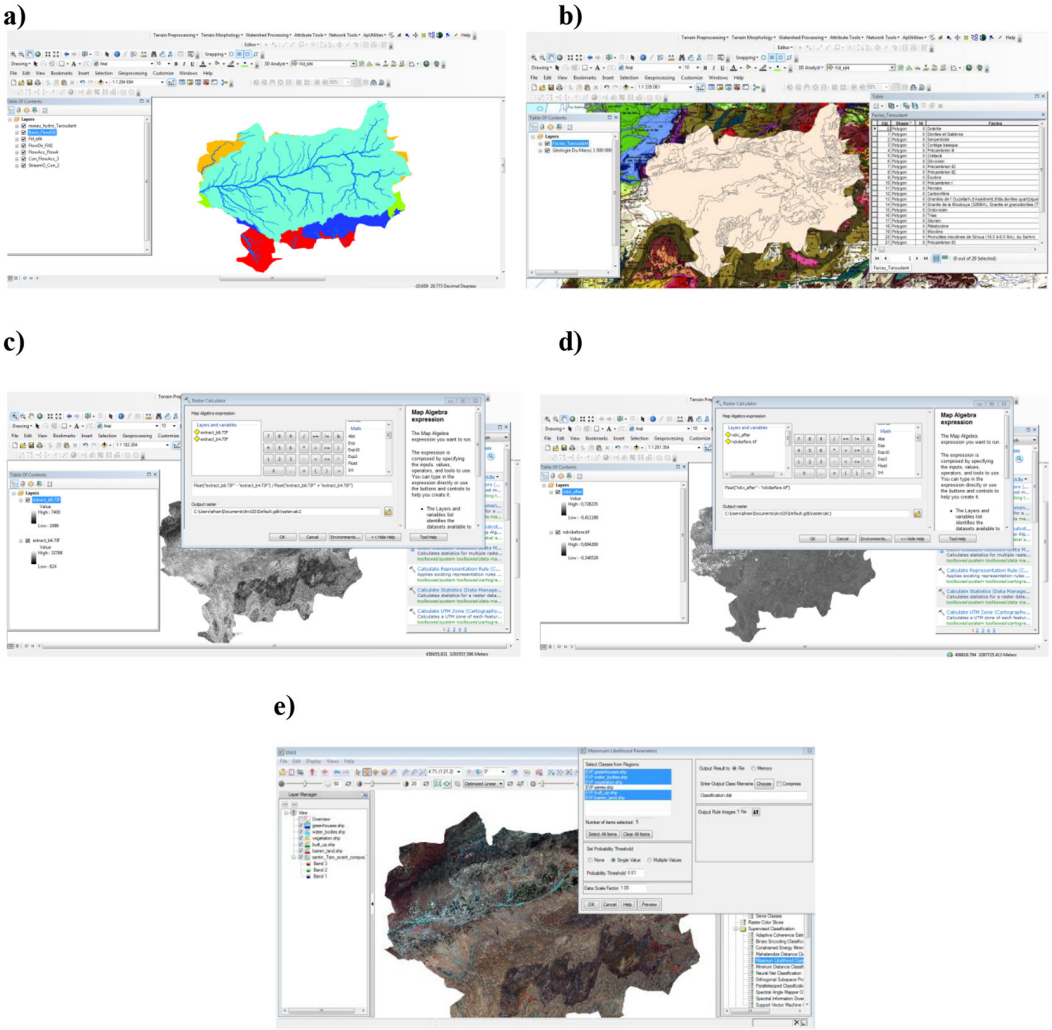

Figure 2. Stages of the study: Manual digitalization of lithological facies (a), Hydrographic network and watershed boundarie (b), NDVI map(c), difference map (d), supervised classification (e)

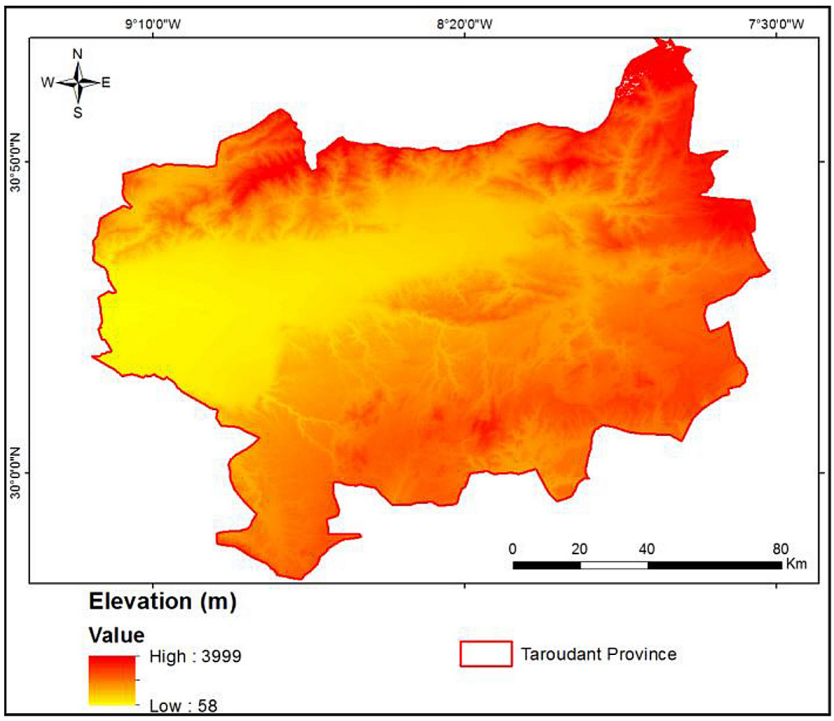

Figure 3. Altitude variation

Geological context

The geological formations found in the Taroudant region belong to three structural domains: the Souss plain in the centre and two Atlas domains (the Anti-Atlas to the south and south-east of the province of Taroudant and the High Atlas to the north-east of the province). Given the lithostratigraphic differences between these structural domains (Figure 4), it is necessary to examine them separately.

The Anti-Atlas

The sedimentary cover of the Precambrian formations of the Anti-Atlas consists of a thick series of carbonate rocks. From bottom to top, we find:

- Infracambrian (terminal Precambrian): limestones, schists and dolomites;
- Georgian (Lower Cambrian): limestone at the base ending in a series of schistose sandstones;
- Acadian and Ordovician: these form an impermeable series of schists.

The High Atlas

The Hercynian massif consists of impermeable crystalline rocks, schists and quartzites several thousand metres thick, with the rest being permeable (conglomerates, sandstones, marls, marl-limestones, etc.).

The Souss Plain

The plain represented by the Souss formation, which consists of fluvial-lacustrine, marl-limestone, clayey and sandstone deposits with conglomerate intercalations.

Lineaments in the area are abundant, with fractures distributed throughout the province. Their orientation, length, and density exhibit significant spatial variability. NE-SW trending lineaments are the most dominant, as indicated by the map, and they are generally the longest. The analysis of rock fracturing is crucial, as fractures largely govern both permeability and porosity, thereby enhancing vertical water flow. Moreover, they provide valuable insights for identifying potential zones suitable for groundwater storage.

Surface water resources

The province's terrain consists of a vast plateau that makes up most of the Souss plain, bordered by the western formations of the Anti-Atlas mountains, which give rise to a large number of watercourses that form the region's hydrographic network (Figure 5).

The main collector of this network is the Souss river, fed by tributaries of varying importance, namely: Issen, Iouziwa, El Ouaar, Bni M'hmed, Lamdad, and Zagmouzen

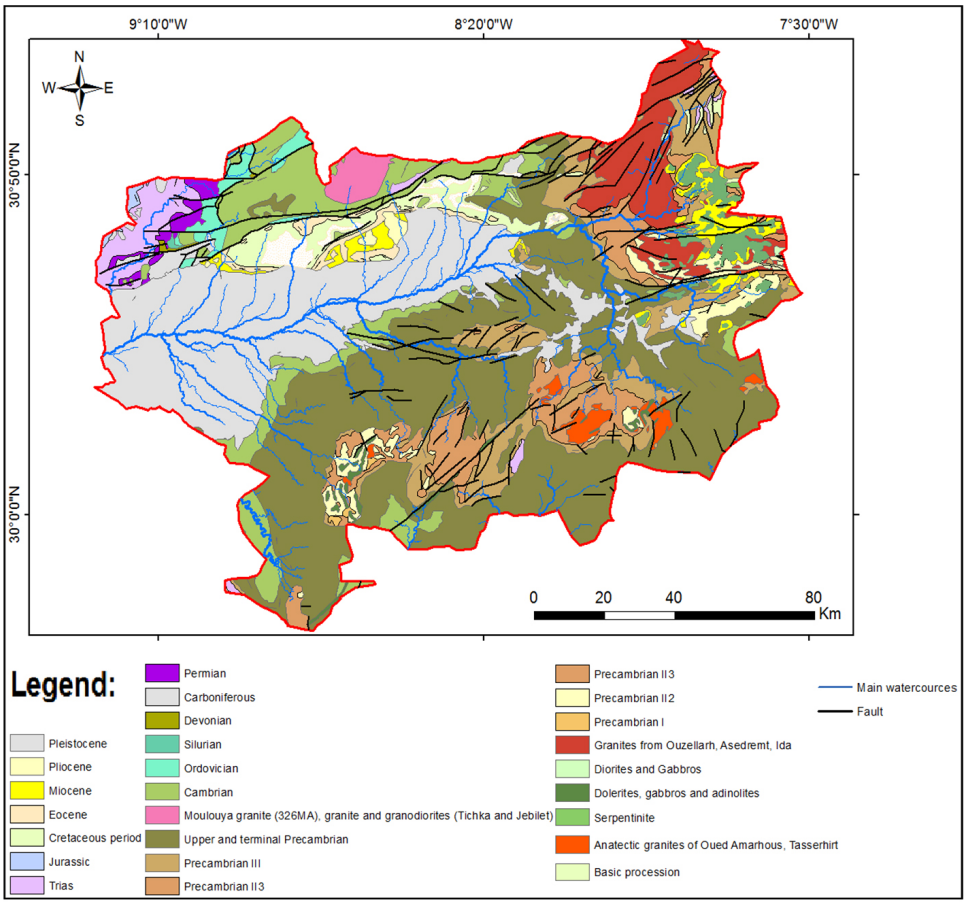

Figure 4. Geological map of the study area

Existing hydraulic installations – the main works carried out on the Souss River are as follows:

- Dams – the province of Taroudant has the following five dams as shown in Table 1, two of which are used for water supply in the Wilaya of Agadir (CSEC, 2001);
- Hill lakes – there are two hill lakes used for livestock watering, irrigation and groundwater recharge – Slaouen (capacity 150 000 m³) and Asedrem (capacity 66 000 m³).

Groundwater

The water resources of the province of Taroudant come from the following reservoirs:

The Souss plain

The unconfined aquifer is the main water resource in the multi-layer system of the Souss plain. It is continuous, mainly in a heterogeneous Pliocene-Quaternary fill limited by a substrate with variable lithostratigraphy (Figure 6), which is represented by geological cross-sections (Figure 7) created based on geophysical data and drilling in the Souss plain (Hsissou, 1999).

The general flow of the aquifer is from east to west (Figure 8) towards the Atlantic Ocean, which is the main outlet for the aquifer.

The High Atlas

Most of the Hercynian mountain range is made up of impermeable terrain, but it does have some formations that store water reservoirs: Cambrian limestone, igneous and metamorphic rocks. These reservoirs are never very large.

The Triassic, which is widely exposed in the Oued Issen valleys, is impermeable; only sandstone can act as aquifers in some areas.

With the exception of the Upper Lias (dolomitic limestone), the entire Lower and Middle Jurassic is of continental origin and impermeable. The Upper Jurassic consists of alternating marl, limestone and marl-limestone. The aquifers are located in the Callovo-Oxfordian marl-limestone and limestone (20 to 50 m thick), the Rauratian-Séquanian limestone (up to 60 m) and the Portlandian limestone (70 to 80 m).

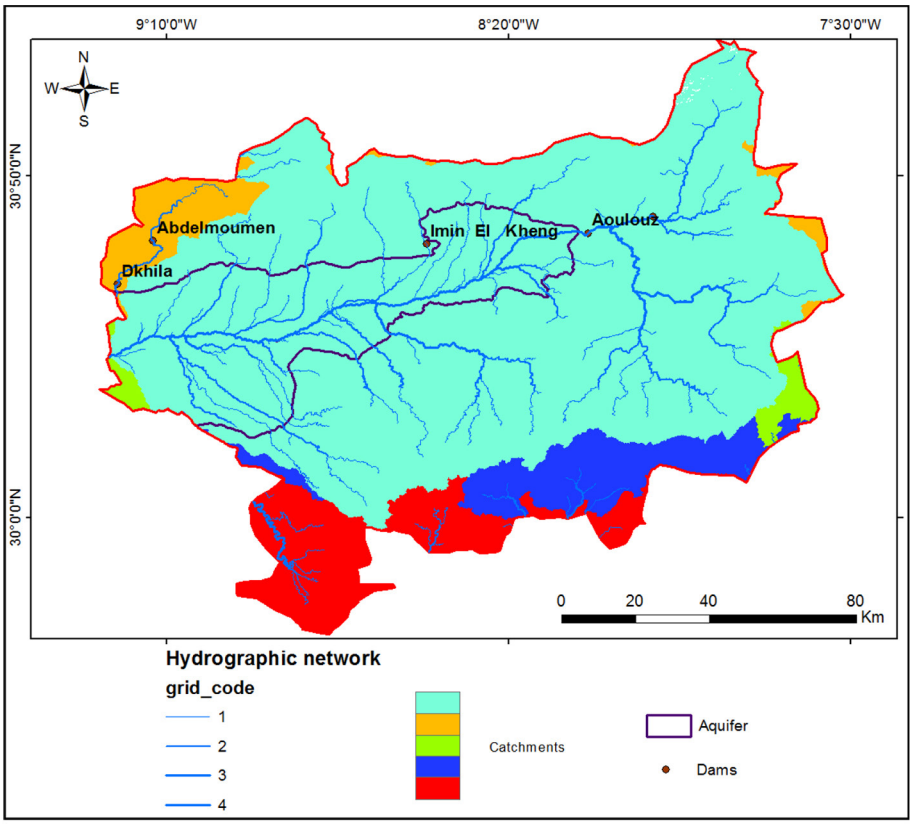

Figure 5. Surface water resources of the study area

Table 1. Existing dams in the province of Taroudant

Dams	Wadi	Year of completion	Capacity (hm^3)
Abdel Moumen	Issen	1 981	214
Dkhila	Issen	1 986	0.7
Aoulouz	Souss	1 991	110
Imin Elkheng	Ibourk	1 993	12
Moukhtar Soussi	Awzioua	2 000	50

Water resources in this region are scarce, mainly superficial and distributed across several temporary wadis fed by rainfall or snowmelt. Potential groundwater is generally consumed locally.

Anti-Atlas

The Adoudounian and Georgian limestones are by far the most interesting given their thickness and catchment area, which enable them to play a major role in regulating groundwater.

The water from these formations most often emerges in the form of small springs at the level of:

- The reddish purple schist series between the Adoudounian and Georgian formations. These are either overflows from the limestones or spills from the upper limestones;
- The terminal limestones of the Georgian formation.

Analysis of the earthquake in al haouz region

Compared to other Mediterranean countries, Morocco is affected by a moderate seismic activity, which is mostly caused by the convergence of Africa and Eurasia. Nonetheless, the population experiences earthquakes every year, which occasionally result in significant local damage. The devastating earthquakes of Agadir, which claimed 12,000 lives, and Al Hoceima, which claimed 629 lives, are still in our memory (Cherkaoui et al., 2010).

On 8 September 2023, a magnitude 6.8 earthquake struck the High Atlas Mountains in western

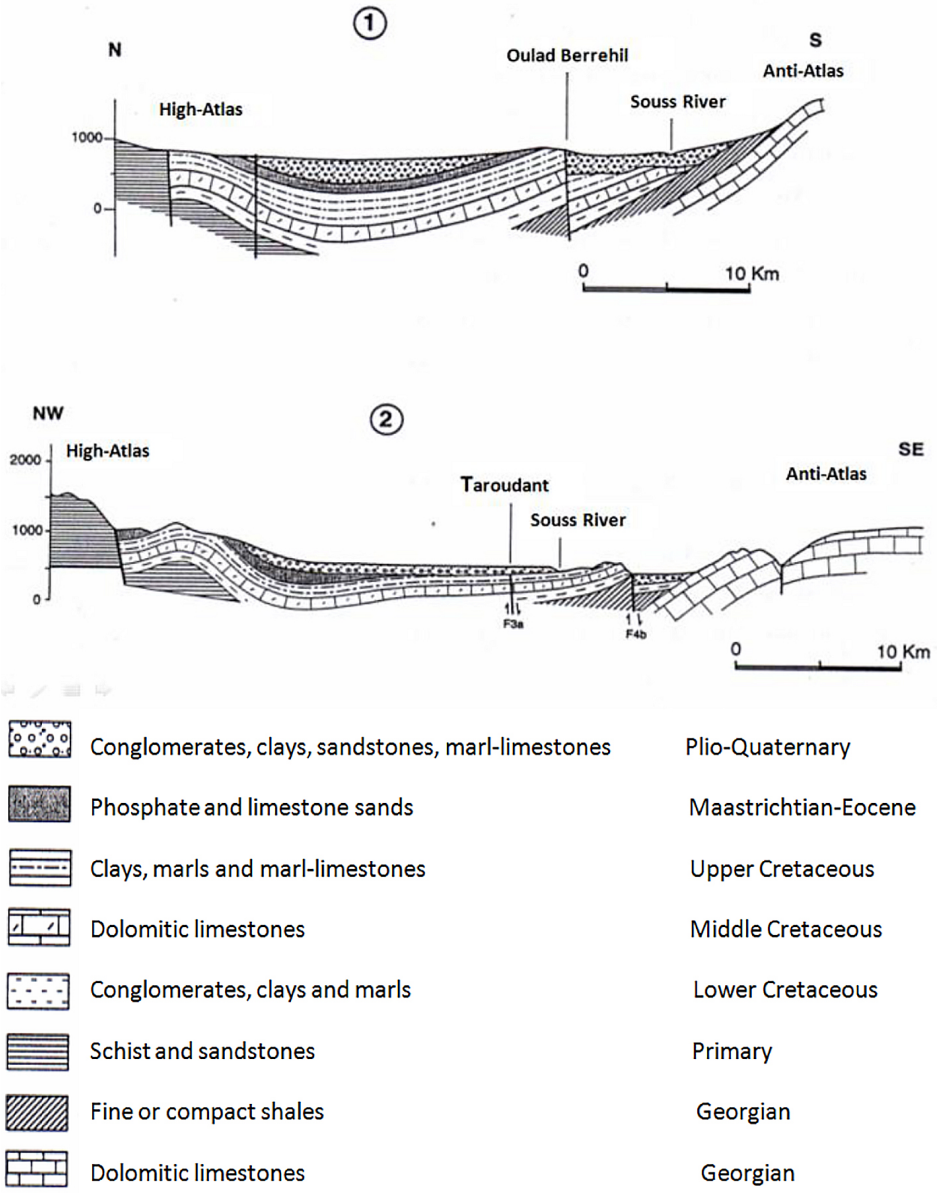

Figure 6. Lithostratigraphy of the Souss plain (Hsissou, (1999), modified)

Morocco, approximately 70 km south-west of Marrakesh (Figure 9), causing significant destruction and loss of life.

According to the High Commission for Planning, The earthquake caused a profound tragedy for Morocco. Nearly 3.000 lives were lost and 4.661 people were injured. In addition to causing significant material damage, the impact resulted in the collapse of 59,674 buildings, 32% of which were totally destroyed and 68% of which were substantially damaged. The Moroccan government responded to this situation by launching an ambitious five-year restoration plan that is expected to cost 120 billion Moroccan dirhams (MAD). The programme aims to improve agricultural and tourism activities, rehabilitate urban areas.

An initial evaluation of the earthquake's effects is included in this policy analysis, with a particular focus on the provinces most impacted: Al Haouz, Taroudant, Chichaoua, and Ouarzazate.

These areas affected by the earthquake are characterised by a predominantly mountainous topography, located in the High Atlas region, covering a total area of 53,135 Km^2. It includes one prefecture 5 provinces, spread over 4 adjacent regions: the provinces of Al Haouz and Chichaoua, the prefecture of Marrakech in the Marrakech-Safi region; the province of Ouarzazate in the Drâa-Tafilalet region; the province of Taroudant in the Souss-Massa region; and the province of Azilal in the Béni Mellal-Khénifra region (Eduardo et al., 2024).

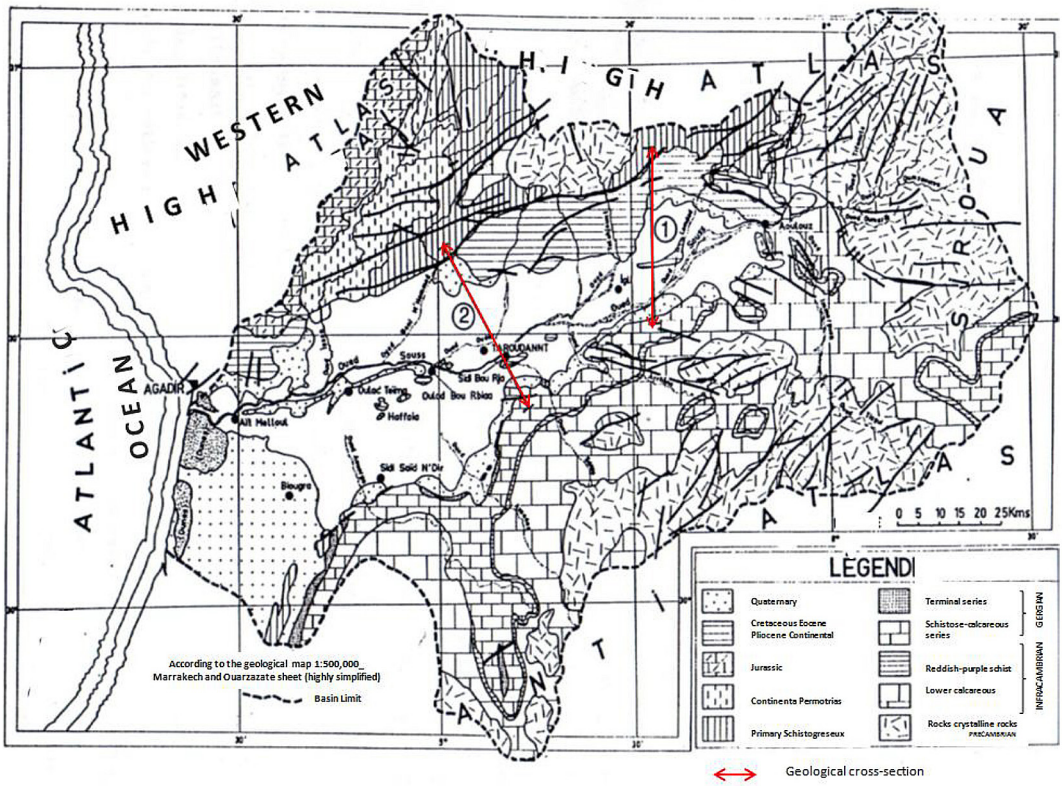

Figure 7. Geological map of the Souss Basin (Hsissou, 1999, modified)

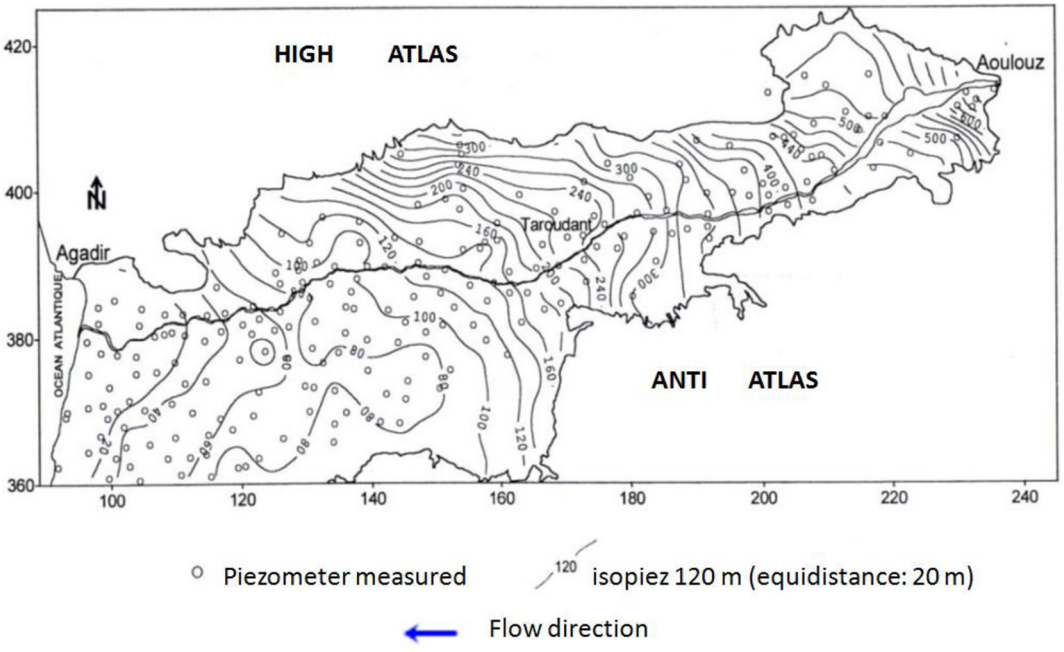

Figure 8. Piezometric map of the Souss aquifer – July 1996 (Hsissou, 1999, modified)

According to the High Commission for Planning, the impact of the earthquake on 8 September 2023 varies considerably from one region to another (Figure 10). Al Haouz was severely affected, with 40 municipalities affected, representing 100% of the region. Chichaoua and Marrakech also suffered damage, with 32 and 13 municipalities affected respectively, and damage rates of 91% and 68%. The province of Ouarzazate was severely impacted, with 17 municipalities affected, representing 100% of the total, while in Taroudant province, the earthquake affected 57

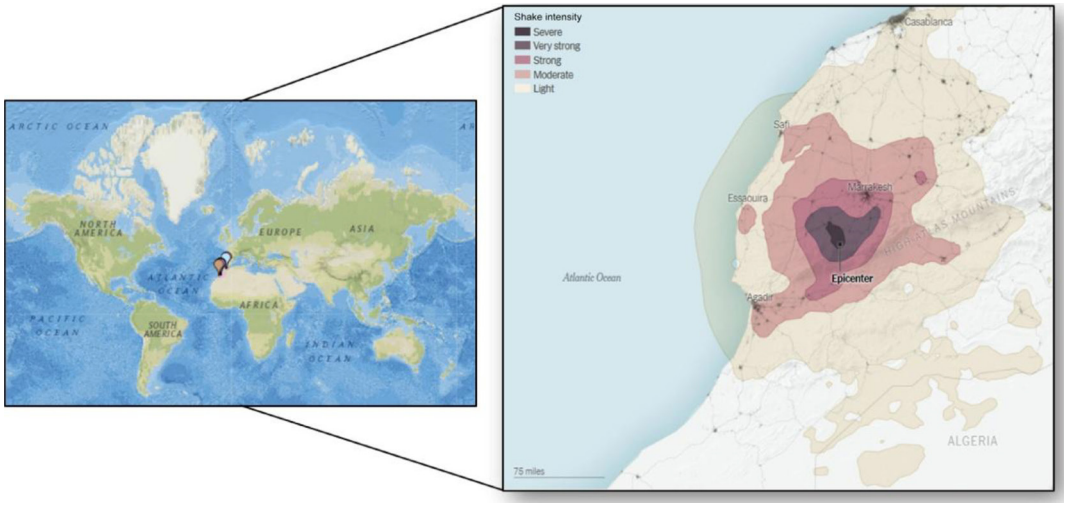

Figure 9. Location of the Al Haouz earthquake (www.maxapress.com)

municipalities, with a damage rate of 64%. Finally, the earthquake affected all 10 municipalities in the province of Azilal, with a damage rate of 23%.

These differences showed how crucial it was to modify each province's rehabilitation and risk-reduction plans in order to reduce the effects of the earthquake.

Descriptive of the changes in the souss-massa region following the earthquake of September 8, 2023

The NDVI vegetation index

NDVI can quantify green vegetation. It normalizes green leaf scattering in Near Infra-red wavelengths with chlorophyll absorption in red wavelengths. The value range of the NDVI is -1 to 1. Negative values of NDVI correspond to water. Values close to zero generally correspond to barren areas of rock, sand, positive values represent shrub and grassland, while high values indicate healthier and denser vegetation.

NDVI images (Figure 11a, Figure 11b) representing the amount of vegetation present at each time. Examining a grayscale of the NDVI for each period was a visually simplistic way to analyze the progression of vegetation, re-growth area and the remover field area or planting field over the two periods. In the results, areas with healthy vegetation are green while areas that are yellow (little or no vegetation), and areas where the vegetation don't exists are orange. The green area which represents vegetated areas has stronger near-infrared reflectance. This means that most of the visible light was used for product biomass thereby producing NDVI values ranging between 0.2 and 1. This represents regions of plants with good condition, high leaf biomass, canopy closure, and vegetation with high chlorophyll content (Sader et al., 1992; Sellers, 1985; Wang et

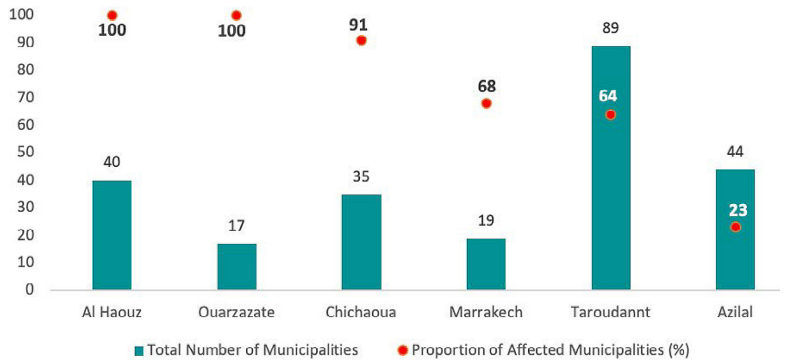

Figure 10. The number and percentage of municipalities affected by disasters by province (High Commission for Planning)

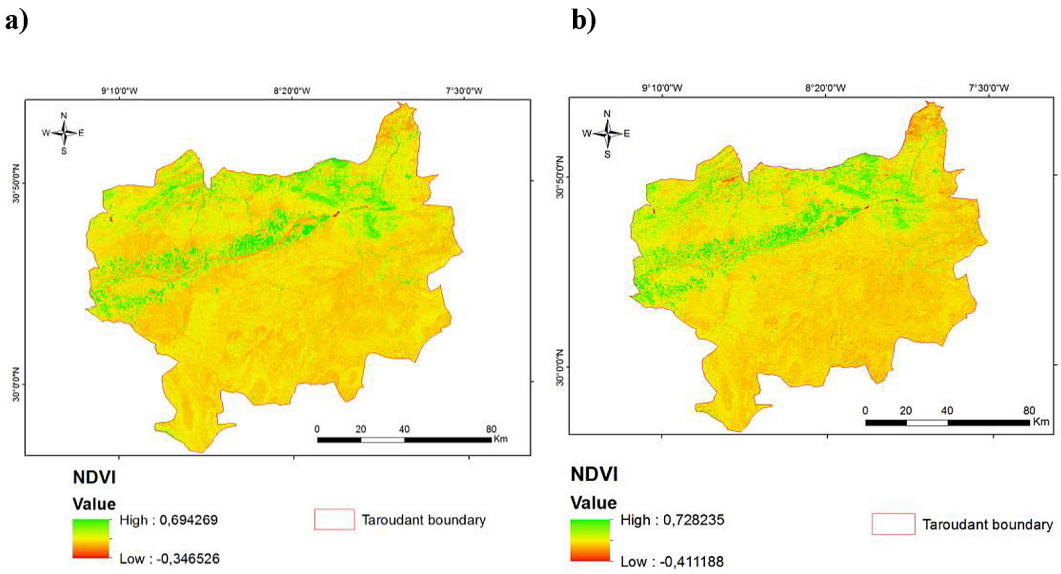

Figure 11. NDVI maps of Taroudant province (a) before and (b) after the earthquake

al., 2004). On the other hand, a yellow and orange region had negative NDVI values. This is because features that indicate areas of low vegetation, typical water, clouds, bare soil, and rock reflect more in the visible band than in the near-infrared spectrum (Lillesand et al., 2004; Crippen, 1990).

The differences between the vegetated areas and un-vegetated areas can be clearly seen in (Figure 12). In the DNDVI image identify the changes that are assigned in red and green colors, while areas with little or no changes are shown in gray color. Likewise, red areas are regions that have a decrease in vegetation and green areas represent an increase in vegetation. The main positive changes or increase in NDVI values between the two periods (pre and post-earthquake) are in the agricultural areas around the Souss River.

The result shows an overall decrease in the amount of vegetation in the north part of Taroudant province and an evolution around the Souss-river.

The normalized difference water index (NDWI)

The NDWI images (Figure 13a, Figure 13b) used to monitor changes related to water content in water bodies. As water bodies strongly absorb light in visible to infrared electromagnetic spectrum, NDWI uses green and near infrared bands to highlight water bodies (Gao, 1996).

Higher index values usually correspond to water bodies. Vegetation usually corresponds to much smaller values and built-up areas to values between zero and 0.2.

This study aimed to model the spatiotemporal changes of water bodies in Taroudant province. Through a comparative analysis, the NDWI was selected and employed for this purpose. The results (Figure 14) showed a significantly increasing trend in the water area after the earthquake (blue areas).

Mapping land cover changes

The classification maps (Figure 15a, Figure 15b) were generated for the two periods (pre- and post-earthquake). These maps are not very useful without quantitative statements about their accuracy. The accuracy evaluation process was done using confusion matrix which were observed in

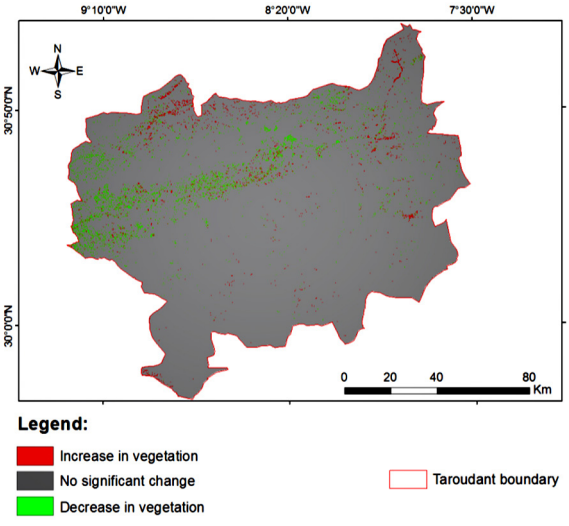

Figure 12. The DNDVI image

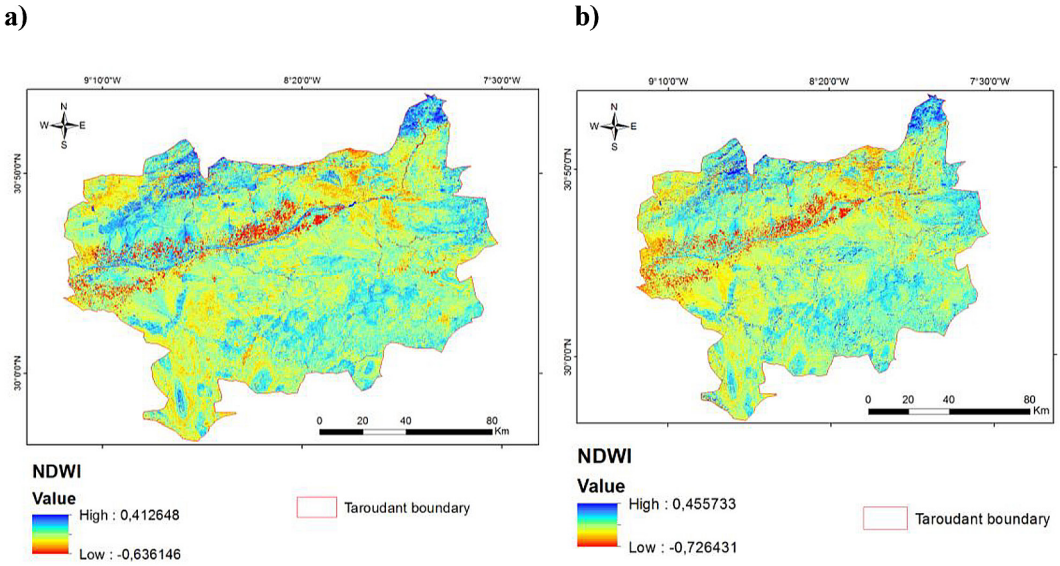

Figure 13. NDWI maps of Taroudant province (a) before and (b) after the earthquake

Table 2 and Table 3. The overall accuracy and the kappa coefficient obtained using maximum likelihood classification for the pre-earthquake image classification are 89. 8% and 0.81, while in the post-eartquake image classification, 80. 65% and 0.66 were obtained.

According to the overall accuracy and the kappa coefficient values, the classification of land cover obtained is good and can be used in the study.

The results summarized in the Table 4 show the class areas and change statistics for the two periods, it can be observed that the water increased by approximately 828.08 km^2, and there is a moderate vegetation decrease from 246.41 km^2. In contrast, greenhouses did not change a lot, but it was an increase in this classe of 16.963 km^2, while the greatest increase was in built-up class of about 76.78 km^2, with the highest decrease occurring in bare-land class of 435.68 km^2.

Most of no vegetation (bare land) was changed to Water bodies or built-up area and the planted areas are at risk of losing vegetation because of climate change and landslides.

Analysis of the relationship between the study area's changing land cover and seismic hazards

The analysis of the results in Section reveals that the vegetation in the study area showed a decreasing trend between 2023 and 2024, which was due to the shift from vegetation to other land cover types caused by the earthquake and its secondary hazards such as landslides, this one destroyed the vegetation at higher altitude and left the ground surface bare. In addition, the increase in built-up area, which is due to the ongoing rehabilitation and reconstruction process within the framework of the relocation program implemented in accordance with royal directives to support areas affected by the earthquake.

Moreover, Normalized Difference water index and spatial distribution of land cover show an increasing trend of water due to the extrusion and expansion of the fracture zone. The fragile terrain of Taroudant is influenced by the Al Haouz earthquake, as seismic activity can cause fractures in geological layers, allowing groundwater to rise to

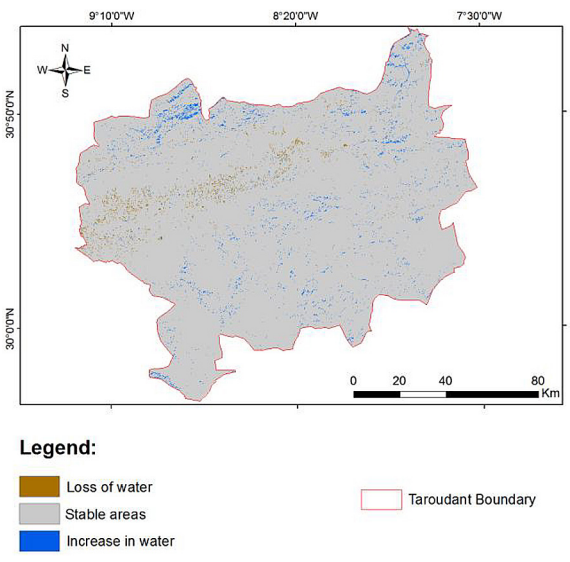

Figure 14. The DNDWI image

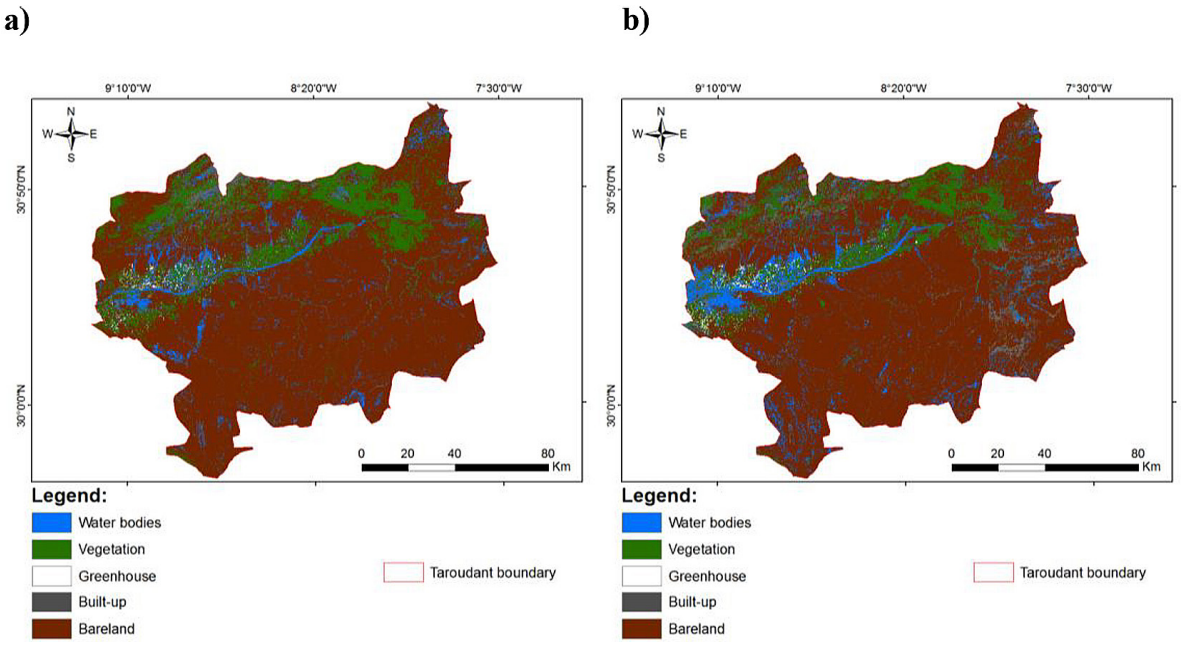

Figure 15. Spatial distribution of land cover in the study area (a) before and (b) after the earthquake

Table 2. Confusion matrix of the pre-earthquake and the post-earthquake

Class	Water bodies	Vegetation	Greenhouses	Built-up	Bare land
Water bodies	89.24	2.72	2.22	5.91	8.20
Vegetation	0.26	93.42	0.10	0.30	0.89
Greenhouses	0.00	1.25	97.60	0.00	0.00
Built-up	3.36	0.21	0.00	86.05	0.50
Bare land	7.14	2.40	0.00	7.73	90.41
Total	100.00	100.00	100.00	100.00	100.00

Table 3. Confusion matrix of the pre-earthquake image classifications: Ground truth (Percent)

Class	Water bodies	Vegetation	Greenhouses	Built-up	Bare land
Water bodies	84.46	1.56	4.30	21.61	12.53
Vegetation	0.35	87.51	0.23	0.60	2.24
Greenhouses	0.00	5.08	95.47	0.00	0.00
Built-up	6.89	0.05	0.00	70.32	9.01
Bare land	8.30	5.80	0.00	7.47	76.22
Total	100.00	100.00	100.00	100.00	100.00

Table 4. Land cover change area in Km^2

Class	Area pre-earthquake (km^2)	Area post-earthquake (km^2)
Water bodies	929.76	1 757.84
Vegetation	2 276.45	2 030.04
Greenhouses	50.207	67.17
Built-up	423.26	500.04
Bare land	12 156.32	11 720.64
Total	16 287.86	16 075.73

the surface or feed new springs. It can also redirect groundwater tables which is the case in the province of Taroudant, where 19 springs were identified, including those at Tizi n'test (Figure 16a), Jbel Tigouga (Figure 16b) and Tifingoult (Figure 16c).

Following the Al Haouz earthquake, the Taroudant province exhibited significant hydrological changes, including the resurgence of

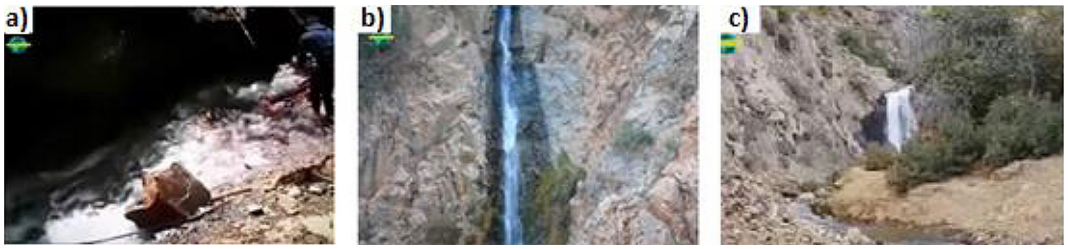

Figure 16. Appearance of a water source at: (a) Tizi n'test, (b) Jbel Tigouga, (c) Tifingoult

multiple springs and an increase in river discharge after several years of drought. These shifts have facilitated the revitalization of agricultural activities that had previously been abandoned due to declining rainfall and long-term climate stressors. Moreover, the emergence of new water sources has potential socio-economic implications, including the promotion of local tourism and the creation of livelihood opportunities for rural populations. Collectively, these transformations indicate that seismic events can temporarily alter hydrogeological conditions, thereby influencing both ecosystem dynamics and regional development trajectories.

The application of remote sensing and GIS proved essential for detecting and monitoring these environmental changes. Multi-temporal satellite imagery enabled rapid mapping of land cover distribution across the affected region, while integrated GIS analysis supported the quantification of post-seismic landscape transformations. Compared with traditional field-based surveys, this approach allowed for efficient, large-scale monitoring, providing timely information critical for post-disaster management, land-use planning, and the assessment of recovery processes (Contreras et al., 2016).

However, several limitations were identified. Cloud cover and atmospheric disturbances can reduce the temporal resolution and accuracy of satellite observations, particularly in regions affected by post-seismic precipitation or landslides. Classification uncertainty remains a challenge when differentiating spectrally similar land cover types, which can partially constrain quantitative analyses. Additionally, remote sensing techniques primarily provide information on surface characteristics and are limited in capturing structural damage to infrastructure, road networks, or population distribution – actors that are critical for disaster mitigation and emergency response planning.

Despite these constraints, the combination of remote sensing and GIS offers a robust framework for rapid environmental assessment and dynamic monitoring in earthquake-affected regions. When integrated with complementary field and socio-economic data, these tools can inform sustainable land management, disaster preparedness, and regional planning strategies that capitalize on emergent natural resources while mitigating future seismic risks.

CONCLUSIONS

This study presents the first high-resolution, multi-temporal assessment of land cover and water resource changes in the Taroudant province following the September 8, 2023 earthquake, using an integrated remote sensing and GIS approach. The post-seismic analysis revealed quantifiable transformations: vegetation decreased by 11% due to landslides and prolonged climatic stress, built-up areas expanded by 18% reflecting reconstruction and rehabilitation activities, and water bodies increased, including the emergence or reactivation of 19 springs, indicating substantial reorganization of the hydrogeological network.

The findings demonstrate that integrating satellite-based land cover mapping with geological and hydrogeological datasets allows accurate evaluation of earthquake-induced environmental changes. This information can directly inform post-disaster management, environmental restoration, and sustainable land-use planning. In particular, identifying areas with increased vulnerability, such as built-up regions on unconsolidated soils or slopes, enables targeted interventions to reduce future seismic risks.

Long-term monitoring of land cover and hydrological parameters, combined with predictive modeling, is recommended to anticipate the impacts of future earthquakes and to guide the design of resilient land-use strategies adapted to local geophysical conditions. The methods and results presented here provide a concrete, evidence-based framework for rapid assessment

of earthquake impacts, supporting both territorial resilience and the sustainable development of disaster-affected regions.

REFERENCES

1. Anderson, J. R., Hardy, E. E., Roach, J. T., Witmer, R. E. (1976). *A land use and land cover classification system for use with remote sensor data*. U.S. Geological Survey Professional Paper 964. Washington, DC: United States Government Printing Office. https://doi.org/10.3133/pp964
2. Canters, F. (1997). Evaluating the uncertainty of area estimates derived from fuzzy land-cover classification. *Photogrammetric Engineering & Remote Sensing, 63*(4), 403–414.
3. Cherkaoui, T. E., El Hassani, A. (2012). Seismicity and seismic hazard in Morocco (1901–2010). In *Proceedings of the International Conference on Seismic Hazard.* 47–55.
4. Clark, M. L., Aide, T. M., Grau, H. R., Riner, G. (2010). A scalable approach to mapping annual land cover at 250 m using MODIS time series data: A case study in the Dry Chaco ecoregion of South America. *Remote Sensing of Environment, 114*(12), 2816–2832. https://doi.org/10.1016/j.rse.2010.07.001
5. Contreras, D., Blaschke, T., Tiede, D., Jilge, M. (2016). Monitoring recovery after earthquakes through the integration of remote sensing, GIS, and ground observations: The case of L'Aquila (Italy). *Cartography and Geographic Information Science, 43*(2), 115–133. https://doi.org/10.1080/15230406.2015.1029520
6. Crippen, R. E. (1990). Calculating the vegetation index faster. *Remote Sensing of Environment, 34*(1), 71–73. https://doi.org/10.1016/0034-4257(90)90085-Z
7. CSEC (Higher Council for Water and Climate). (2001). *Master plan for the development of water resources in the Souss-Massa basins*. Agadir, Morocco.
8. Haddad, E. A., El Aynaoui, K., Ait Ali, A., Arbouch, M., Saoudi, H., Araujo, I. F. (2024). Assessing the economic impacts of the Al-Haouz earthquake: Damages and recovery strategy.
9. Gao, B. C. (1996). NDWI – A normalized difference water index for remote sensing of vegetation liquid water from space. *Remote Sensing of Environment, 58*(3), 257–266. https://doi.org/10.1016/S0034-4257(96)00067-3
10. Hsissou, Y. (1999). *Impact of the natural and anthropogenic environment on the quality of alluvial waters in semi-arid areas: The case of the Souss plain (Morocco)* (Doctoral dissertation). Ibn Zohr University.
11. Lillesand, T. M., Kiefer, R. W., Chipman, J. W. (2004). *Remote sensing and image interpretation* (5th ed.). John Wiley & Sons.
12. Sader, S. A., Winne, J. C. (1992). RGB-NDVI colour composites for visualizing forest change dynamics. *International Journal of Remote Sensing, 13*(16), 3055–3067. https://doi.org/10.1080/01431169208904101
13. Sellers, P. J. (1985). Canopy reflectance, photosynthesis and transpiration. *International Journal of Remote Sensing, 6*(8), 1335–1372. https://doi.org/10.1080/01431168508948283
14. Tung, F., LeDrew, E. (1988). The determination of optimal threshold levels for change detection using various accuracy indexes. *Photogrammetric Engineering & Remote Sensing, 54*(10), 1449–1454.
15. Walker, R. (2004). Theorizing land-cover and land-use change: The case of tropical deforestation. *International Regional Science Review, 27*(3), 247–270. https://doi.org/10.1177/0160017604266026
16. Wang, J., Rich, P. M., Price, K. P., Kettle, W. D. (2004). Relations between NDVI and tree productivity in the central Great Plains. *International Journal of Remote Sensing, 25*(16), 3127–3138. https://doi.org/10.1080/0143116032000160499